Copyright © 2013 Tech Science Press CMES, vol.96, no.4, pp.243-257, 2013

Efficient BEM Stress Analysis of 3D Generally Anisotropic Elastic Solids With Stress Concentrations and Cracks

Y.C. Shiah[1], C.L. Tan[2] and Y.H. Chen[3]

Abstract: The present authors have recently proposed an efficient, alternative approach to numerically evaluate the fundamental solution and its derivatives for 3D general anisotropic elasticity. It is based on a double Fourier series representation of the exact, explicit form of the Green's function derived by Ting and Lee (1997). This paper reports on the successful implementation of the fundamental solution and its derivatives based on this Fourier series scheme in the boundary element method (BEM) for 3D general anisotropic elastostatics. Some numerical examples of stress concentration problems and a crack problem are presented to demonstrate the veracity of the implementation. The results of the BEM analysis of these problems show excellent agreement with those obtained using the commercial finite element code ANSYS and with known analytical solutions in all cases.

Keywords: Anisotropic elasticity, Green's function, Fourier series, stress concentrations, fracture mechanics.

1 Introduction

The boundary element method (BEM) is well established as an efficient computational tool for three-dimensional (3D) linear elastic stress analysis of isotropic bodies. It is, however, significantly less so for treating 3D generally anisotropic elastic solids. The primary reason lies in the relatively slow progress made over the years for an efficient means to numerically evaluate the fundamental solution (or Green's function) and its derivatives for this class of problems. These quantities are necessary items in the development of the boundary integral equation (BIE) which is the analytical basis of the BEM.

[1] Corresponding author, Dept. of Aeronautics and Astronautics, National Cheng Kung University, Tainan 701, Taiwan, R.O.C.

[2] Dept. of Mechanical & Aerospace Engineering, Carleton University, Ottawa, Canada K1S 5B6

[3] Dept. of Computer Science & Information Management, Providence University, Taichung, Taiwan, R.O.C.

The Green's function, $\mathbf{U}(\mathbf{x})$, for a 3D anisotropic medium as first derived by Lifschitz and Rosenzweig (1947) is expressed as a line integral around a unit circle with the integrand containing the Christoffel matrix defined in terms of elastic constants. Since then, there have been numerous efforts to reformulate it into simpler or more explicit analytical forms, including those carried out in the context of BEM development [see, e.g. Synge (1957); Barnett (1972); Nakamura and Tanuma (1997); Wang (1997); Pan and Yuan (2000); Tonon and Pan (2001)]. In the pioneering work of Wilson and Cruse (1978), a large database of the fundamental solution is generated in advance for a given material from direct numerical computations of the Lifschitz and Rozentsweig's solution, and an interpolation scheme is used in their BEM implementation. The efficiency and accuracy of this scheme have been called into question for highly anisotropic materials and various other schemes to this end have been proposed for use in BEM [see, e.g. Sales and Gray (1998); Phan et al (2004); Wang and Denda (2007)].

Of significance to note here is that Ting and Lee (1997) have derived a fully algebraic, explicit form of the 3D anisotropic Green's function, expressed in terms of Stroh's eigenvalues. Lee (2003, 2009) further showed how its derivatives could be obtained; the complete explicit expressions for the derivatives for general anisotropy were, however, derived and presented only by the present authors and their coworkers in Shiah et al (2008) and Shiah et al (2010). They were also implemented in Tan et al (2009) to analyse some benchmark problems by the BEM. Also, Shiah and Tan (2011) have analytically derived the higher-order derivatives, expressed as explicit closed-forms. In their attempts to develop less elaborate forms of this $\mathbf{U}(\mathbf{x})$ and its derivatives to facilitate efficient numerical evaluation of these quantities, the present lead authors have very recently [Shiah et al (2012a)] proposed that advantage can be taken of the periodic nature of the spherical angles if $\mathbf{U}(\mathbf{x})$ is expressed in spherical coordinates. This allows the Green's function to be represented by a double Fourier series and its derivatives can also be obtained in a straightforward manner by direct differentiation of the series. Not only are the resulting formulations significantly more concise, a very important advantage is that the evaluation of the coefficients of the Fourier series is performed only once, regardless of the number of field points involved in the BEM analysis. This makes the scheme very efficient indeed without any sacrifice in accuracy. To further enhance the computational efficiency, the authors [Shiah et al (2012b) and Tan et al (2013)] reformulated the scheme by organizing and simplifying the terms, and taking advantage of some of the characteristics of the Fourier series, so that less number of terms needs to be summed. This has implications for the efficiency of the numerical algorithm in the BEM analysis, noting too that slightly more refined meshes are typically needed when treating, for example, 3D stress concentration and cracked

problems of anisotropic bodies than of isotropic ones. The reformulated Fourier series scheme for $\mathbf{U}(\mathbf{x})$ and its derivatives have been implemented into an existing BEM code for 3D general anisotropic elasticity. Some examples involving stress concentrations and a crack problem is presented in this paper to demonstrate this and the accuracy of the solutions obtained. Before this, a review of the approach is in order.

2 BIE and fundamental solutions of 3D anisotropic elastic bodies

The boundary integral equation (BIE) that relates the displacements, u_i, to the tractions, t_i, on the surface S of the domain can be expressed in indicial notation as

$$C_{ij}\,u_i(P) + \int_S u_i(Q)\,T_{ij}(P,Q)dS = \int_S t_i(Q)\,U_{ij}(P,Q)dS \tag{1}$$

In Eq.(1), $U_{ij}(P,Q) \equiv \mathbf{U}(\mathbf{x})$ and $T_{ij}(P,Q)$ represent the fundamental solutions of displacements and tractions, respectively, in the x_i-direction at the field point Q due to a unit load in the x_j-direction at P in a homogeneous infinite body; also, $C_{ij}(P)$ depends on the geometry of the surface at P. The numerical evaluation of $\mathbf{U}(\mathbf{x})$ for generally anisotropic materials proposed by Ting and Lee (1997) has been discussed by Shiah et al (2008). Nevertheless, it is useful to first provide a brief review.

With reference to Fig.1, let n and m be two mutually perpendicular unit vectors on the oblique plane at Q normal to the position vector $\mathbf{x}$; the vectors [$\mathbf{n}$, $\mathbf{m}$, $\mathbf{x}/r$] forms a right-angle triad.

By considering a spherical coordinate system as shown, the explicit form of the Green's function can be expressed as

$$\mathbf{U}(\mathbf{x}) = \frac{1}{4\pi \mathrm{r}} \frac{1}{|\boldsymbol{\kappa}|} \sum_{\mathrm{n}=0}^{4} \mathrm{q_n} \hat{\mathbf{\Gamma}}^{(\mathrm{n})} \quad , \tag{2}$$

where r represents the radial distance between the source point P and the field point Q; q_n, $\hat{\mathbf{\Gamma}}^{(\mathrm{n})}$, and $\boldsymbol{\kappa}$ are given by [Shiah et al (2008)]

$$\mathrm{q_n} = \begin{cases} \frac{-1}{2\beta_1\beta_2\beta_3}\left[\mathrm{Re}\left\{\sum_{\mathrm{t}=1}^{3} \frac{\mathrm{p_t^n}}{(\mathrm{p_t}-\bar{\mathrm{p}}_{\mathrm{t}+1})(\mathrm{p_t}-\bar{\mathrm{p}}_{\mathrm{t}+2})}\right\} - \delta_{\mathrm{n}2}\right] for \mathrm{n} = 0, 1, 2, \\ \frac{1}{2\beta_1\beta_2\beta_3}\mathrm{Re}\left\{\sum_{\mathrm{t}=1}^{3} \frac{\mathrm{p_t^{n-2}}\bar{\mathrm{p}}_{\mathrm{t}+1}\bar{\mathrm{p}}_{\mathrm{t}+2}}{(\mathrm{p_t}-\bar{\mathrm{p}}_{\mathrm{t}+1})(\mathrm{p_t}-\bar{\mathrm{p}}_{\mathrm{t}+2})}\right\} for \mathrm{n} = 3,\ 4, \end{cases} \tag{3a}$$

$$\hat{\Gamma}^{(\mathrm{n})}_{\mathrm{ij}} = \tilde{\Gamma}^{(\mathrm{n})}_{(i+1)(j+1)(i+2)(j+2)} - \tilde{\Gamma}^{(\mathrm{n})}_{(i+1)(j+2)(i+2)(j+1)}, \quad (\mathrm{i,j} = 1,\ 2,\ 3) \tag{3b}$$

$$\kappa_{\mathrm{ik}} = \mathrm{C_{ijks}} \mathrm{m_j} \mathrm{m_s}, \quad \mathbf{m} = (-\sin\theta,\ \cos\theta,\ 0) \tag{3c}$$

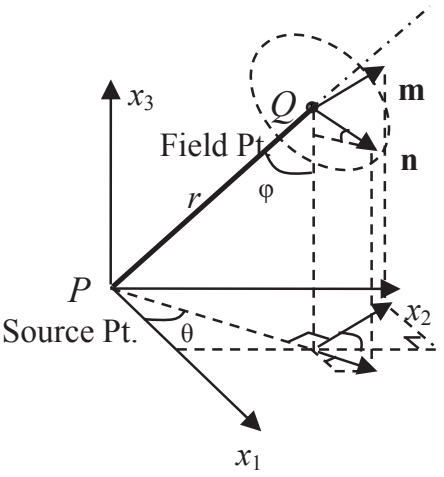

Figure 1: Vectors definitions in the spherical coordinate system.

In Eq.(3a), the Stroh eigenvalues, p_i, are the roots of the sextic equation, obtained by setting $|\boldsymbol{\kappa}|$ equal null and β_i are the positive imaginary parts of p_i; in Eq.(3b), $\tilde{\boldsymbol{\Gamma}}$ are defined as follows:

$$\begin{aligned}
&\tilde{\Gamma}^{(4)}_{pqrs} = \kappa_{pq}\kappa_{rs},\ \tilde{\Gamma}^{(3)}_{pqrs} = V_{pq}\kappa_{rs}+\kappa_{pq}V_{rs},\\
&\tilde{\Gamma}^{(2)}_{pqrs} = \kappa_{pq}W_{rs}+\kappa_{rs}W_{pq}+V_{pq}V_{rs},\\
&\tilde{\Gamma}^{(1)}_{pqrs} = V_{pq}W_{rs}+V_{rs}W_{pq},\ \tilde{\Gamma}^{(0)}_{pqrs} = W_{pq}W_{rs},
\end{aligned} \tag{4}$$

where $\mathbf{W}$, $\mathbf{V}$ are given by

$$W_{ik}=C_{ijks}n_jn_s, V_{ik}=(C_{ijks}+C_{kjis})n_jm_s \tag{5}$$

In the above equations, C_{ijks} are the stiffness coefficients of the anisotropic material. It has already been shown [Shiah et al (2008); Tan et al (2009)] that the direct computation of Eq.(2) for $\mathbf{U}(\mathbf{x})$ is relatively straightforward and very efficient indeed. Lee (2003) and Shiah et al (2008) have also obtained the analytical expressions for the derivatives of $\mathbf{U}(\mathbf{x})$. They are in terms of some very high order tensors and although direct to evaluate, is found to be the best form for computations. This is re-examined by Lee (2009), who showed that the very high order tensors can be avoided by differentiating $\mathbf{U}(\mathbf{x})$ with respect to spherical coordinates as an intermediate step, separating the terms associated with the radial distance, and then using the usual chain rule. This approached was followed in Shiah et al (2010), where explicit expressions for the 1^{st} and 2^{nd} derivatives of $\mathbf{U}(\mathbf{x})$ in general

anisotropy are obtained and implemented in the BEM. Although relatively more efficient to compute, their implementation is somewhat tedious because of their lengthy forms.

As an alternative approach for the numerical evaluation of $\mathbf{U}(\mathbf{x})$, the present authors very recently [Shiah et al (2012a)] proposed a Fourier series representation of $\mathbf{U}(\mathbf{x})$ and its derivatives in terms of the spherical coordinates. This scheme yields significantly more concise expressions that can be easily implemented in BEM programming and was shown to be computationally very much more efficient for the evaluation of the Green's function and its derivatives. The Green's function can be expressed in the spherical coordinates as

$$U_{uv}(r,\theta,\phi) = \frac{H_{uv}(\theta,\phi)}{4\pi r}, \quad (u,\ v = 1,\ 2,\ 3) \tag{6}$$

By virtue of its periodical nature, one may further rewrite the H_{uv} in Eq.(6) into a Fourier series, viz.

$$H_{uv}(\theta,\phi) = \sum_{m=-\alpha}^{\alpha} \sum_{n=-\alpha}^{\alpha} \lambda_{uv}^{(m,n)}\, e^{\mathbf{i}(m\theta+n\phi)}, \tag{7}$$

where α is an appropriately large integer for convergence of the series and the unknown Fourier coefficients $\lambda_{uv}^{(m,n)}$ are given by

$$\lambda_{uv}^{(m,n)} = \frac{1}{4\pi^2} \int_{-\pi}^{\pi} \int_{-\pi}^{\pi} H_{uv}(\theta,\phi)\ e^{-\mathbf{i}(m\theta+n\phi)} d\theta\, d\phi. \tag{8}$$

Equation (8) can be numerically determined by, for example the Gaussian quadrature scheme as follows,

$$\lambda_{uv}^{(m,n)} = \frac{1}{4} \sum_{p=1}^{k} \sum_{q=1}^{k} w_p w_q f_{uv}^{(m,n)}(\pi\xi_p, \pi\xi_q), \tag{9}$$

where $f_{uv}^{(m,n)}$ represents the integrand in Eq.(8); k is the number of the Gauss abscissa, ξ_p, and w_p is the corresponding weight. It should be noted that the computation of the Fourier coefficients is performed only once, irrespective of the number of nodes and elements in the BEM mesh; the CPU time for this evaluation is trivial indeed in a complete BEM analysis. To reduce the number of terms truly required in the series for the computations, Tan et al (2013) separated $\lambda_{uv}^{(m,n)}$ into its real part $R_{uv}^{(m,n)}$ and imaginary part $I_{uv}^{(m,n)}$ as follows,

$$\lambda_{uv}^{(m,n)} = R_{uv}^{(m,n)} + \mathbf{i}\, I_{uv}^{(m,n)}. \tag{10}$$

and expressed the Green's function as

$$U_{uv} = \frac{1}{2\pi r}\left\{ \begin{array}{l} \sum\limits_{m=1}^{\alpha}\sum\limits_{n=1}^{\alpha}\left[\begin{array}{l} \left(\tilde{R}_{uv}^{(m,n)}\cos m\theta - \tilde{I}_{uv}^{(m,n)}\sin m\theta\right)\cos n\phi \\ -\left(\hat{R}_{uv}^{(m,n)}\sin m\theta + \hat{I}_{uv}^{(m,n)}\cos m\theta\right)\sin n\phi \end{array} \right] \\ +\sum\limits_{m=1}^{\alpha}\left(\begin{array}{l} R_{uv}^{(0,m)}\cos m\phi - I_{uv}^{(0,m)}\sin m\phi \\ +R_{uv}^{(m,0)}\cos m\,\theta - I_{uv}^{(m,0)}\sin m\theta \end{array} \right) + \frac{R_{uv}^{(0,0)}}{2} \end{array} \right\}, \tag{11}$$

where $\tilde{R}_{uv}^{(m,n)}$, $\hat{R}_{uv}^{(m,n)}$, $\tilde{I}_{uv}^{(m,n)}$, and $\hat{I}_{uv}^{(m,n)}$ are given by

$$\begin{array}{llll} \tilde{R}_{uv}^{(m,n)} = R_{uv}^{(m,n)} + R_{uv}^{(m,-n)}, & \hat{R}_{uv}^{(m,n)} = R_{uv}^{(m,n)} - R_{uv}^{(m,-n)}, \\ \tilde{I}_{uv}^{(m,n)} = I_{uv}^{(m,n)} + I_{uv}^{(m,-n)}, & \hat{I}_{uv}^{(m,n)} = I_{uv}^{(m,n)} - I_{uv}^{(m,-n)}. \end{array} \tag{12}$$

Since no operations of complex numbers are involved and the number of terms in the series is minimized, the numerical computations are very efficient indeed. The derivatives of Eq.(6) can be obtained in a straightforward manner by simply differentiating the Fourier series of U_{uv} as follows,

$$U_{uv,l} = \frac{\partial U_{uv}}{\partial r}\frac{\partial r}{\partial x_l} + \frac{\partial U_{uv}}{\partial \theta}\frac{\partial \theta}{\partial x_l} + \frac{\partial U_{uv}}{\partial \phi}\frac{\partial \phi}{\partial x_l}. \tag{13}$$

This can be shown [Tan et al (2013)] to result in the following form:

$$\begin{aligned} U_{uv,l} = & \frac{-1}{2\pi r^2}\{\omega_l(\theta,\phi)[\sum_{m=1}^{\alpha}\sum_{n=1}^{\alpha}(\bar{\Gamma}_{uv}^{(m,n)}(\theta)\cos n\phi - \bar{\bar{\Gamma}}_{uv}^{(m,n)}(\theta)\sin n\phi) \\ & + \sum_{m=1}^{\alpha}(\overline{\gamma}_{uv}^{m}(\theta) + \bar{\bar{\gamma}}_{uv}^{m}(\phi)) + \frac{R_{uv}^{(0,0)}}{2} \\ & + \omega_l'(\theta,\phi)[\sum_{m=1}^{\alpha}\sum_{n=1}^{\alpha} m(\widetilde{\Gamma}_{uv}^{(m,n)}(\theta)\cos n\phi + \widehat{\Gamma}_{uv}^{(m,n)}(\theta)\sin n\phi) + \sum_{m=1}^{\alpha} m\cdot\widetilde{\gamma}_{uv}^{m}(\theta)] \\ & + \omega_l''(\theta,\phi)[\sum_{m=1}^{\alpha}\sum_{n=1}^{\alpha} n(\overline{\Gamma}_{uv}^{(m,n)}(\theta)\sin n\phi + \bar{\bar{\Gamma}}_{uv}^{(m,n)}(\theta)\cos n\phi) + \sum_{m=1}^{\alpha} m\cdot\widehat{\gamma}_{uv}^{m}(\phi)]\} \end{aligned} \tag{14}$$

where

$$
\begin{aligned}
&\overline{\Gamma}_{uv}^{(m,n)}(\theta) = \tilde{R}_{uv}^{(m,n)} \cos m\theta - \tilde{I}_{uv}^{(m,n)} \sin m\theta,\\
&\overline{\overline{\Gamma}}_{uv}^{(m,n)}(\theta) = \hat{R}_{uv}^{(m,n)} \sin m\theta + \hat{I}_{uv}^{(m,n)} \cos m\theta,\\
&\tilde{\Gamma}_{uv}^{(m,n)}(\theta) = \tilde{R}_{uv}^{(m,n)} \sin m\theta + \tilde{I}_{uv}^{(m,n)} \cos m\theta,\\
&\hat{\Gamma}_{uv}^{(m,n)}(\theta) = \hat{R}_{uv}^{(m,n)} \cos m\theta - \hat{I}_{uv}^{(m,n)} \sin m\theta,\\
&\overline{\gamma}_{uv}^{m}(\theta) = R_{uv}^{(m,0)} \cos m\,\theta - I_{uv}^{(m,0)} \sin m\,\theta,\\
&\overline{\overline{\gamma}}_{uv}^{m}(\phi) = R_{uv}^{(0,m)} \cos m\phi - I_{uv}^{(0,m)} \sin m\phi,\\
&\tilde{\gamma}_{uv}^{m}(\theta) = R_{uv}^{(m,0)} \sin m\,\theta + I_{uv}^{(m,0)} \cos m\,\theta,\\
&\hat{\gamma}_{uv}^{m}(\phi) = R_{uv}^{(0,m)} \sin m\,\phi + I_{uv}^{(0,m)} \cos m\,\phi,\\
&\omega_l(\theta,\phi) = \sin\phi\cos\theta, \quad \omega_l'(\theta,\phi) = -\sin\theta/\sin\phi,\\
&\omega_l''(\theta,\phi) = \cos\phi\cos\theta \quad \text{for} \quad l=1,\\
&\omega_l(\theta,\phi) = \sin\phi\sin\theta, \quad \omega_l'(\theta,\phi) = \cos\theta/\sin\phi,\\
&\omega_l''(\theta,\phi) = \cos\phi\sin\theta \quad \text{for} \quad l=2,\\
&\omega_l(\theta,\phi) = \cos\phi, \qquad \omega_l'(\theta,\phi) = 0,\\
&\omega_l''(\theta,\phi) = -\sin\phi \quad \text{for} \quad l=3.
\end{aligned}
\tag{15}
$$

Compared to the previous exact analytical forms, the above is even simpler to implement into an existing BEM computer code. However, it should be noted that in the above expressions, there is numerical singularity when ϕ=0 or π. This is due to the multi-valued definition of θ when ϕ=0 or π. The details of this are discussed in Tan et al (2013) and the problem may be easily resolved by re-definition of the coordinates. Once the 1^{st}-order derivatives of $\mathbf{U}(\mathbf{x})$ are computed, the fundamental solution of tractions can be determined by

$$T_{ij} = C_{ikmn}\,(U_{mj,n} + U_{nj,m})\,N_k/2, \tag{16}$$

where N_k denotes the components of the unit outward normal vector at the field point. In a similar manner, the derivatives of higher orders may also be derived, but they are not of concern for the study in this paper.

3 Numerical examples

In this section, three example cases are investigated for the study of stress concentrations and fracture by the Fourier series approach. For the present analyses, the series number α=16 and 64 Gauss integration points for computing the Fourier coefficients were used for all the three cases. More

The first example, shown in Fig. 2, is a sphere containing a solid spherical rigid inclusion (R_2/R_1=2). It is subjected to uniform hydrostatic tensile P on its outer surface while the innner surface is fully constrained to the rigid inclusion. An alpha-quartz single crystal is chosen as the material, whose stiffness coefficients, denoted by $\mathbf{C}^*$, are given by [Huntington (1958)]:

$$\mathbf{C}^* = \begin{pmatrix} 87.6 & 6.07 & 13.3 & 17.3 & 0.0 & 0.0 \\ 6.07 & 87.6 & 13.3 & -17.3 & 0.0 & 0.0 \\ 13.3 & 13.3 & 106.8 & 0.0 & 0.0 & 0.0 \\ 17.3 & -17.3 & 0.0 & 57.2 & 0.0 & 0.0 \\ 0.0 & 0.0 & 0.0 & 0.0 & 57.2 & 17.3 \\ 0.0 & 0.0 & 0.0 & 0.0 & 17.3 & 40.765 \end{pmatrix} \text{ GPa.} \tag{17}$$

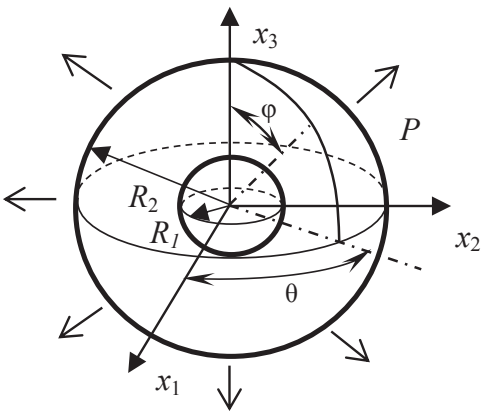

Figure 2: A sphere with a solid conclusion- Example 1

For demonstrating the capability of the approach in dealing with general anisotropy, the material principal axes are arbitrarily rotated with respect to the x_1-, x_2- and x_3-axis by -20°, 55°, and 145°, respectively, with positive rotation angles being defines in the conterclockwise direction. This results in the material stiffness matrix defined in the global Cartesian coordinates as

$$\mathbf{C} = \begin{pmatrix} 102.22 & 10.90 & -1.16 & -3.39 & -7.76 & 20.08 \\ 10.90 & 114.23 & -4.39 & 13.87 & -3.57 & -11.79 \\ -1.16 & -4.39 & 120.20 & -0.19 & 17.52 & -0.01 \\ -3.39 & 13.87 & -0.19 & 37.77 & 2.88 & -1.42 \\ -7.76 & -3.57 & 17.52 & 2.88 & 37.95 & 0.19 \\ 20.08 & -11.79 & -0.01 & -1.42 & 0.19 & 52.12 \end{pmatrix} \text{ GPa.} \tag{18}$$

For the BEM analysis, 240 quadratic isoparametric elements with 644 nodes were employed. For verification, the problem was also analysed by ANSYS, using 61440 SOLID186 elements with 70092 nodes. Figure 3 shows the mesh discretisations of the BEM full model and a partial (one-eighth) ANSYS FEM model for the sake of clarity.

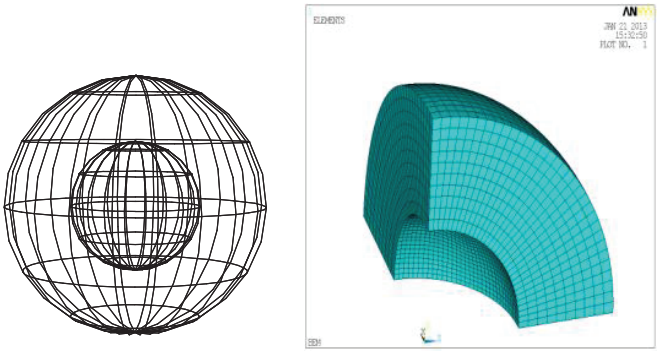

Figure 3: Mesh discretisations of the BEM and ANSYS- Example 1

The computed variations of the normalised hoop and meridional stress, $\sigma_{\theta\theta}/\sigma_0$ and $\sigma_{\phi\phi}/\sigma_0$, at the inner and outer radius around the equator in the $x_1 - x_2$ plane are shown in Figure 4. It can be seen that the BEM results are in excellent agreement with those obtained from the FEM analysis by ANSYS. As expected, the fluctuations of the stress concentrations are more evident on the inner surface. Both analyses were carried out and clocked on a PC-based computer equipped with quad-core Intel CPU; the runs recorded 43.96 seconds and 27 minutes for the BEM and ANSYS operations, respectively.

The second example considered is an ellipsoidal cavity in a cylindrical bar, as shown in Figure 5. Three values of the aspect ratio, R_2/R_1, as defined in the figure, are considered, namely, 1.0, 2.0, and 3.0. The radius of the cylindrical bar R_0=10R_1 is taken and its length is $2R_0$. The bar is subjected to axial tension σ_0 at one end and is fully constrained at the other. The same material properties as in the previous example are used again for the analysis. Also shown in Fig.5 is the BEM full model, where 216 quadratic elements were employed. For verification, the problem was also analysed by ANSYS, using 216934 SOLID187 elements.

Due to the relatively large dimension of the cylinder as compared with the size of the ellipsoid, this case actually approximates an infinite anisotropic domain with an ellipsoidal cavity when it is subjected to a remote uniaxial tension. The variations of calculated stress concentration factor (SCF), defined by σ_{33}/σ_0, around

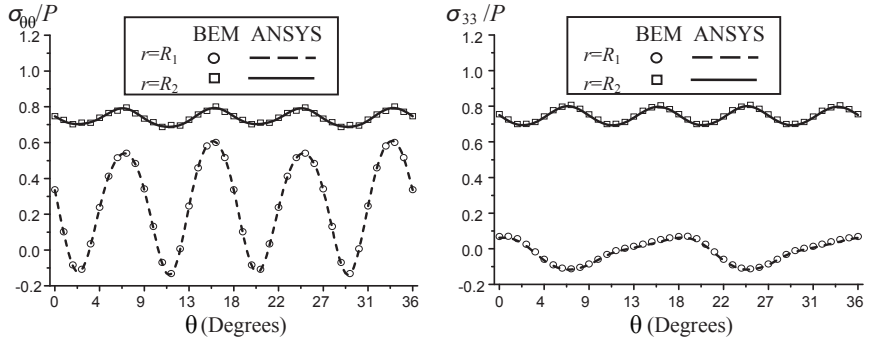

Figure 4: Normalized hoop stresses along the equator on the $x_1 - x_2$ plane

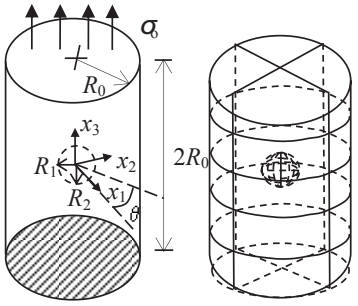

Figure 5: An ellipsoidal cavity in a cylinder subjected to uniaxial tension- Example 2

the surface of the ellipsoidal cavity at x_3=0 are shown in Fig.6, where again, excellent agreement between the two sets of results from the BEM and FEM analyses is achieved. The cpu times recorded for the BEM and ANSY analysis were 32.65 seconds and 26 minutes, respectively.

The last example treated here is a penny-shaped crack in an infinite transversely isotropic medium; it is a special case of anisotropy. It has also been has been studied using BEM by Tan el al (2010), and the exact solutions for the stress intensity factors (SIFs) under different load conditions are available. More fracture problems treating cracks with different degrees of complexity can be referred to Dong and Atluri (2013a, 2013b), where the SGBEM-FEM alternating method was employed. For the material of the present problem, a graphite-epoxy composite with

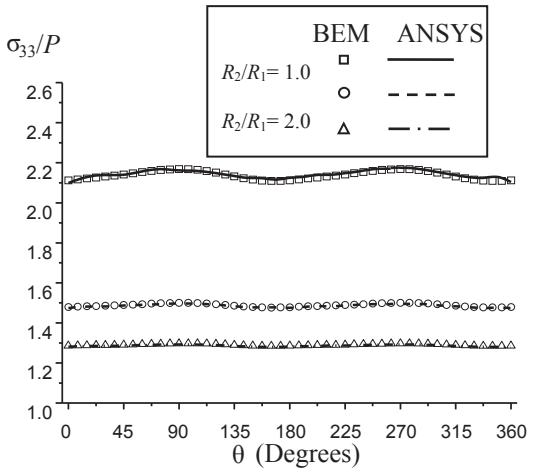

Figure 6: Stress concentration on the equator surface of the ellipsoid

the following stiffness coefficients [Saez et al (1997)] is considered:

$$\begin{aligned} &C_{11} = 13.92 \text{ MPa}, C_{12} = 6.92 \text{ MPa}, C_{13} = 6.44 \text{ MPa}, \\ &C_{33} = 160.7 \text{ MPa}, C_{44} = 7.07 \text{ MPa}. \end{aligned} \tag{19}$$

Two load cases are treated, namely, (i) remote uniform tension of $\sigma_{33} = \sigma_o$ and (ii) remote shear stress $\sigma_{23} = \tau_o$, applied at the top and bottom faces of the cube modelled. For the BEM analysis, the body is modelled as a cube with side lengths ten times the diameter, $2a$, of the crack which lies on the mid-plane; this is shown in Fig.7. Although advantage can be taken of the planes of symmetry, the full problem was modelled as the mesh will be used for more general case of loading and anisotropy in other studies. Special $O(r^{-1/2})$ traction-singular crack-front elements are employed and the SIFs are obtained using the computed traction coefficients at the crack-front nodes using the well-established "traction-formula" [Luichi and Rizzuti (1987)], as follows:

$$(K_I)_A = (t_3^*)_A \sqrt{\pi l}\,, \quad (K_{II})_A = (t_1^*)_A \sqrt{\pi l}\,, \quad (K_{III})_A = (t_2^*)_A \sqrt{\pi l}\,, \tag{20}$$

In Eq.(20), $(t_i^*)_A$ are the traction coefficients computed at the crack-front node A of the traction-singular element and l is the width of this element. The width of the crack-front element for this case was set to be $l/a = 0.15$.

For case (i), the exact solution for the normalized stress intensity factor, $K_I/\sigma_o\sqrt{\pi a}$, is 0.637. The BEM result computed using the traction formula is 0.638, with an error less than 1%. For load case (ii), the exact normalized SIFs for the material

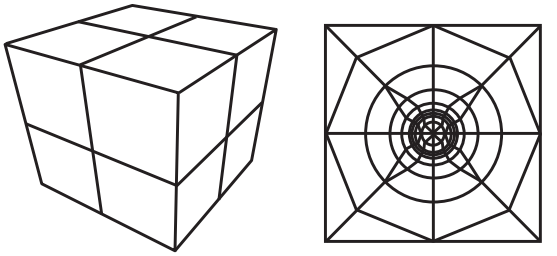

Figure 7: BEM mesh for Example 3; 216 elements, 604 nodes

Table 1: Computed normalised SIFs at various angular positions for Example 3

θ (Deg.)	$K_{II}/\tau_o\sqrt{\pi a}$			$K_{III}/\tau_o\sqrt{\pi a}$		
	Exact	BEM	|Error %|	Exact	BEM	|Error %|
0	0.0000	0.0000	N/A	0.4617	0.4566	1.10
15	0.2100	0.2097	0.03	0.4459	0.4422	0.83
30	0.4057	0.4042	0.15	0.3999	0.3954	1.12
45	0.5738	0.5740	0.02	0.3264	0.3237	0.83
60	0.7016	0.7004	0.17	0.2309	0.2284	1.08
75	0.7838	0.7842	0.05	0.1194	0.1185	0.75
90	0.8115	0.8087	0.35	0.0000	0.0000	N/A

properties used in the analysis are $[K_{II}/\tau_o\sqrt{\pi a} = 0.8115\sin\theta\,,\ K_{III}/\tau_o\sqrt{\pi a} = 0.4617\cos\theta\,]$; the angle θ here is the angular position measured from the x_1-axis. Table 1 lists all computed SIFs of case (ii) for various angular positions

It can be seen that the SIFs calculated by the BEM using the Fourier approach agree with the exact solutions with the maximum error of 1.12%.

4 Conclusions

The efficient evaluation of the fundamental solutions is critical to the success of the BEM as a numerical tool for treating three-dimensional generally anisotropic bodies. Very recently, the lead authors (2012) presented an efficient scheme to compute the fundamental solutions, where the Green's function and its derivatives are represented by a Fourier series; a modification to the scheme was also very recently [Tan et al (2013)] developed to reduce the number of calculations required in the series summation. This revised Fourier series scheme for the evaluation of the Green's

function has been implemented into a BEM code for three-dimensional anisotropic elasticity. The success of this implementation has been demonstrated in this paper by two examples in stress concentrations where the results are compared with those obtained by FEM. Excellent agreement of the results have been obtained while requiring significantly less computational effort. A fracture problem has also been presented and the BEM results when compared with the exact analytical solutions again showed very good agreement indeed.

Acknowledgement: The authors gratefully acknowledge the financial support from the National Science and Engineering Research Council of Canada and the National Science Council of Taiwan (NSC 102-2221-E-006-290-MY3).

References

Barnett, D. M. (1972): The precise evaluation of derivatives of the anisotropic elastic Green's functions. *Phys. Stat. Sol. (b),* vol. 49, pp. 741–748.

Dong, L.; Atluri, S. N. (2013a): Fracture & Fatigue Analyses: SGBEM-FEM or XFEM? Part 1: 2D Structures. *CMES: CMES-Comp. Modeling Eng. & Sci.*, vol. 90, no. 2, pp. 91-146.

Dong, L.; Atluri, S. N. (2013b): Fracture & Fatigue Analyses: SGBEM-FEM or XFEM? Part 2: 2D Structures. *CMES: CMES-Comp. Modeling Eng. & Sci.*, vol. 90, no. 7, pp. 379-413.

Huntington, H.B. (1958): *The Elastic Constants of Crystal*. Academic Press, New York.

Lee, V. G. (2003): Explicit expression of derivatives of elastic Green's functions for general anisotropic materials. *Mech. Res. Comm.*, vol. 30, pp. 241–249.

Lee, V. G. (2009): Derivatives of the three-dimensional Green's function for anisotropic materials. *Int. J. Solids Struct.*, vol. 46, pp. 1471-1479

Lifshitz, I. M.; Rozenzweig, L. N. (1947): Construction of the Green Tensor for the fundamental equation of elasticity theory in the case of unbounded elastically anisotropic medium. *Zh. Eksp. Teor. Fiz.*, vol. 17, pp. 783-791.

Luichi, M. L.; Rizzuti, S. (1987): Boundary elements for three-dimensional elastic crack analysis. *Int. J. Numer. Methods Engng*., vol. 24, no. 12, pp. 2253-2271.

Nakamura, G.; Tanuma, K. (1997): A formula for the fundamental solution of anisotropic elasticity. *Q. J. Mech. Appl. Math.*, vol. 50, pp. 179-194.

Pan, E.; Yuan, F. G. (2000): Boundary element analysis of three dimensional cracks in anisotropic solids. *Int. J. Numer. Methods Engng.*, vol. 48, pp. 211-237.

Phan, P. V.; Gray, L. J.; Kaplan, T. (2004): On the residue calculus evaluation of

the 3D anisotropic elastic Green's function. *Comm. Numer. Methods Engng.*, vol. 20, pp. 335-341.

Saez, A.; Ariza, M. P.; Dominguez, J. (1997): Three-dimensional fracture analysis in transversely isotropic solids. *Engng. Analysis Boundary Elem.*, vol. 20, pp. 287-298.

Sales, M. A.; Gray, L. J. (1998): Evaluation of the anisotropic Green's function and its derivatives. *Comp. & Struct.*, vol. 69, pp. 247-254.

Shiah, Y. C.; Tan, C. L.; Lee, V. G. (2008): Evaluation of explicit-form fundamental solutions for displacements and stresses in 3D anisotropic elastic solids. *CMES-Comp. Modeling Eng. & Sci.*, vol. 34, pp. 205-226.

Shiah, Y. C.; Tan, C. L.; Lee, R. F. (2010): Internal point solutions for displacements and stresses in 3D anisotropic elastic solids using the boundary element method. *CMES-Comp. Modeling Eng. & Sci.*, vol. 69, pp. 167-197.

Shiah, Y. C.; Tan, C. L. (2011): Higher-order Green's function derivatives and BEM evaluation of stresses at interior points in a 3D generally anisotropic solid. *CMES-Comp. Modeling Eng. & Sci.*, vol. 78, pp. 95-108.

Shiah, Y. C.; Tan, C. L.; Wang, C. Y. (2012a): Efficient Computation of the Green's Function and its Derivatives for Three-Dimensional Anisotropic Elasticity in BEM Analysis. *Engng. Analysis Boundary Elem.*, vol. 36, pp. 1746-1755.

Shiah, Y. C.; Tan, C. L.; Wang, C. Y. (2012b): An Improved Numerical Evaluation Scheme of the Fundamental Solution and its Derivatives for 3D Anisotropic Elasticity Based on Fourier Series. *CMES-Comp. Modeling Eng. & Sci.*, vol. 87, no. 1, pp. 1-22.

Synge, J. L. (1957): *The Hypercircle in Mathematical Physics*. Cambridge University Press, Cambridge

Tan, C. L.; Shiah, Y. C.; Lin, C. W. (2009): Stress Analysis of 3D Generally Anisotropic Elastic Solids Using the Boundary Element Method. *CMES-Comp. Modeling Eng. & Sci.*, vol. 41, pp. 195-214.

Tan, C. L.; Shiah, Y. C.; Armitage, J. R.; Hsia, W. C. (2010): BEM Fracture Mechanics Analysis of 3D Generally Anisotropic Solids. *Advances in Boundary Element Techniques XI*, pp. 468-473, Eds. C.H. Zhang, M.H. Aliabadi, M. Schanz, Berlin, Germany, 12-14 July.

Tan, C. L.; Shiah, Y. C.; Wang, C. Y., (2013): Boundary Element Elastic Stress Analysis of 3D Generally Anisotropic Solids Using Fundamental Solutions Based on Fourier Series. *Int. J. Solids Struct.*, vol. 50, pp. 2701-2711.

Ting, T. C. T.; Lee, V. G. (1997): The three-dimensional elastostic Green's function for general anisotropic linear elastic solid. *Q. J. Mech. Appl. Math.*, vol. 50,

pp. 407-426.

Tonon, F.; Pan, E.; Amadei, B. (2001): Green's functions and boundary element method formulation for 3D anisotropic media. *Comp. & Struct.*, vol. 79, pp. 469-482.

Wang, C. Y. (1997): Elastic fields produced by a point source in solids of general anisotropy. *J. Engng. Math.*, vol. 32, pp. 41-52.

Wang, C. Y.; Denda, M. (2007): 3D BEM for general anisotropic elasticity. *Int. J. Solids Struct.*, vol. 44, pp. 7073-7091.

Wilson, R. B.; Cruse, T. A. (1978): Efficient implementation of anisotropic three dimensional boundary integral equation stress analysis. *Int. J. Num. Methods Engng.*, vol. 12, pp. 1383-1397.